Parathymosin Affects the Binding of Linker Histone H1 to Nucleosomes and Remodels Chromatin Structure*

Goran Martic‡§, Zoe Karetsou‡, Katerina Kefala‡, Anastasia S. Politou‡, Cedric R. Clapier¶, Tobias Straub‖, and Thomais Papamarcaki‡**‡‡

*From the ‡Laboratory of Biological Chemistry, Medical School, University of Ioannina, 451 10 Ioannina, Greece, the ¶EMBL Grenoble Outstation, BP181 38042 Grenoble Cedex 9, France, the ‖Adolf-Butenandt-Institute, Molecular Biology, Schillerstrasse 44, 80336 Munich, Germany, and the **Foundation for Research and Technology-Hellas/Biomedical Research Institute, 451 10 Ioannina, Greece*

Linker histone H1 is the major factor that stabilizes higher order chromatin structure and modulates the action of chromatin-remodeling enzymes. We have previously shown that parathymosin, an acidic, nuclear protein binds to histone H1 *in vitro* and *in vivo*. Confocal laser scanning microscopy reveals a nuclear punctuate staining of the endogenous protein in interphase cells, which is excluded from dense heterochromatic regions. Using an *in vitro* chromatin reconstitution system under physiological conditions, we show here that parathymosin (ParaT) inhibits the binding of H1 to chromatin in a dose-dependent manner. Consistent with these findings, H1-containing chromatin assembled in the presence of ParaT has reduced nucleosome spacing. These observations suggest that interaction of the two proteins might result in a conformational change of H1. Fluorescence spectroscopy and circular dichroism-based measurements on mixtures of H1 and ParaT confirm this hypothesis. Human sperm nuclei challenged with ParaT become highly decondensed, whereas overexpression of green fluorescent protein- or FLAG-tagged protein in HeLa cells induces global chromatin decondensation and increases the accessibility of chromatin to micrococcal nuclease digestion. Our data suggest a role of parathymosin in the remodeling of higher order chromatin structure through modulation of H1 interaction with nucleosomes and point to its involvement in chromatin-dependent functions.

Eukaryotic DNA is packaged into chromatin (1), a structural framework that plays a key role in the regulation of the transcriptional status of genes and genetic loci (2–4). The basic level of chromatin organization is the nucleosome that consists of DNA wrapped around an octamer of histones (5). Linker histones (*e.g.* H1 and H5) seal the entry/exit of DNA and stabilize the folding of 10-nm nucleosomal arrays into higher order chromatin structures (6, 7). Binding of histone H1 to nucleosomal arrays affects the spacing of nucleosomes (8), restricts their mobility (9), and reduces the transient exposure of DNA on the nucleosome surface (10). Consistent with its structural role as a major determinant of chromatin folding, histone H1 was found to inhibit the action of enzymes that enhance the accessibility of DNA, such as histone acetyltransferases and ATP-dependent remodeling complexes. For example, changes in linker histone stoichiometry modulate the levels of core histone acetylation (11) and regulate the activity of all classes of ATP-dependent remodeling enzymes (12, 13). Collectively, these findings support the notion that H1 "locks down" chromatin regions and acts as a general inhibitor of transcription (14, 15). However, genetic studies have shown that, rather than being global repressors of transcription, linker histones affect the expression of specific genes (16). Multiple isoforms of linker histone H1 exist in mammalian somatic cells (17) and play differential roles in gene expression (18). Recently, two independent studies highlight the important role of H1 subtypes in development and apoptosis. H1b, a specific subtype of H1, which is expressed in undifferentiated cells, specifically represses the expression of *MyoD* gene, and thus restricts muscle development (19). Furthermore, in response to DNA double-strand breaks, only H1.2 (H1c) translocates from the nucleus into the cytoplasm and triggers the onset of apoptosis through the release of cytochrome *c* from mitochondria (20).

Collectively, the properties of linker histone H1 suggest that local H1 displacement and/or rearrangement must occur for efficient re-organization of chromatin during several DNA-dependent processes. Therefore, the roles of specific H1-protein interactions appear to be important for H1 function and chromatin structure. We have previously reported a specific *in vitro* and *in vivo* interaction between parathymosin (ParaT)[1] and histone H1 (21). ParaT is expressed in all cell types (22) and is widely distributed in mammalian tissues with the highest concentrations found in liver, heart, and kidney (23). It contains a functionally active bipartite nuclear localization signal and is actively translocated into the nuclei of undifferentiated cells (24). Inspection of the amino acid sequence of ParaT (101 amino acids, pI 4.15) reveals that it is predominantly composed of hydrophilic amino acids, typically found on protein surfaces. Aromatic, sulfur, histidine, isoleucine, and leucine amino acids are totally absent, whereas the central region of the protein contains runs of aspartic and glutamic acid residues, occasionally interspersed with glycine, alanine, threonine, and asparagine (25). This unusual sequence shares significant similarity

[1] The abbreviations used are: ParaT, parathymosin; CMV, cytomegalovirus; GFP, green fluorescent protein; TAF, template-activating factor; GST, glutathione *S*-transferase; BSA, bovine serum albumin; PBS, phosphate-buffered saline; TRITC, tetramethyl rhodamine isothiocyanate; CD, circular dichroism; NRL, nucleosome repeat length.

with the amino acid composition of prothymosin α, a histone H1-binding protein associated with cell proliferation, chromatin remodeling, and gene transcription (26–29).

Data on the biological function of ParaT suggest functions in both the cytoplasm and nucleus. Early studies have identified ParaT as a zinc-binding protein, which interacts with several enzymes involved in carbohydrate metabolism (30, 31). Recently, ParaT was found to inhibit the binding of the activated glucocorticoid receptor to nuclei, suggesting its involvement in the regulation of glucocorticoid steroids action (32).

In the present study we analyzed the effect of ParaT on the interaction of histone H1 with chromatin using an *in vitro* chromatin reconstitution system on plasmid and bead-immobilized DNA. We also monitored the binding of H1 and ParaT by circular dichroism and fluorescence spectroscopy to detect potential changes of H1 conformation in the presence of ParaT. Furthermore, we studied the potential involvement of this acidic polypeptide in chromatin decondensation. Our results indicate that ParaT modulates the interaction of histone H1 with chromatin and induces global chromatin decondensation.

MATERIALS AND METHODS

Plasmids—To generate pCMVParaT the coding region of the rat ParaT cDNA (23) was amplified and subcloned into the EcoRI-XhoI sites of a CMV expression cassette p163/7, where the H2 promoter was exchanged with the CMV promoter. For pFLAG-ParaT, the coding region of ParaT was amplified and subcloned into the EcoRI-SalI sites of pFLAG-CMV2 vector (Eastman Kodak Co.). To generate pGST-ParaT, the coding region of the protein was removed from pFLAG-ParaT and cloned into the EcoRI-SmaI sites of pGEX-6P3 (Amersham Biosciences). GFP-ParaT was made by inserting ParaT gene into EcoRI-SmaI cleavage sites of pEGFP-C1 expression vector (Clontech). pFLAG-TAF-Iβ was a gift from Dr. D. C. Tkachuk (VA Puget Sound Health Care System, Seattle, WA). To generate pGFP-TAF-Iβ, the TAF-Iβ gene was cloned into the EcoRI-SalI sites of pEFGP-C3 vector (Clontech). All constructs have been verified by sequencing.

Proteins—ParaT was purified from goat liver by a new method; freshly excised tissue was immediately frozen in liquid nitrogen and stored at −80 °C. Frozen tissue, 60 g, was pulverized in liquid nitrogen and immediately added to 300 ml of boiling water. The suspension was cooled, homogenized with a Polytron homogenizer, and centrifuged at $12,000 \times g$ for 25 min. The supernatant was adjusted to pH 5.0 with 1.0 M of acetic acid and centrifuged at $12,000 \times g$ for 25 min. The new supernatant was concentrated to 12 ml and dialyzed over buffer A (10 mM Tris, pH 7.4, 0.5 mM phenylmethylsulfonyl fluoride, 1 mM EDTA). The sample was incubated for 1 h at 4 °C with DE-52 beads (Whatman) pre-equilibrated with the same buffer and poured into a column. The column was washed with 0.1 M NaCl, and bound proteins were eluted with a linear salt gradient of 0.1–0.7 M NaCl in buffer A. The fractions were checked by SDS-PAGE, and those containing ParaT were pooled, dialyzed over buffer B (20 mM histidine, pH 5.9, 0.5 mM phenylmethylsulfonyl fluoride, 1 mM EDTA), and applied over a Q-Sepharose column previously equilibrated with buffer B. The column was eluted with a linear gradient of 0–1.0 M NaCl in buffer B. ParaT fractions were pooled and filtered through a Sep-Pak cartridge (Waters Associates Inc.). The filter was washed three times with ddH₂O, and ParaT was eluted with 20% isopropanol in ddH₂O. The purity of the ParaT fractions was checked by 15% SDS-PAGE. ParaT concentration was determined by bicinchoninic acid protein determination kit (Pierce). This method yields ~10 μg of pure ParaT/g tissue.

Glutathione *S*-transferase (GST)-ParaT was expressed in BL21 cells and purified from lysates according to standard procedures (33). The binding of recombinant ParaT to H1 was checked by GST-pull-down assays at 500 mM salt concentration. To remove the GST moiety, GST-ParaT was immobilized on glutathione beads and digested with the PreScission Protease (Amersham Biosciences), 2 units of enzyme/100 μg of bound GST-ParaT in 20 μl of cleavage buffer (50 mM Tris-HCl, pH 7.0, 150 mM NaCl, 1 mM EDTA, 1 mM dithiothreitol, 0.1% Nonidet P-40) at 4 °C for 12 h.

Peptide P1 (residues 5–30) was synthesized at Hoffmann-La Roche, Nutley, NJ, according to the published sequence of rat ParaT (34) and used as an antigen for antibody production. Histone H1 from calf thymus (Roche Molecular Biochemicals) was phosphorylated with pro-

tein kinase C in the presence of 20 μCi of [γ-³²P]ATP, 50 μM ATP, 0.2% BSA, 1% phospholipids, for 30 min at 37 °C.

Chromatin Reconstitution—Chromatin assembly extract was prepared from *Drosophila* early embryos (35). Plasmid immobilization on paramagnetic beads and chromatin assembly reactions were performed as described previously (36). To incorporate H1 into chromatin, 2 units of H1 was mixed with assembly extract prior to the addition of DNA beads. Chromatin was assembled for 6 h at 25 °C, and beads were concentrated in a magnetic field. Immobilized chromatin was washed with 650 mM NaCl to strip bound H1, then three times with 100 mM NaCl, and finally equilibrated in the binding buffer (20 mM Tris-HCl, 100 mM NaCl, 1 mM MgCl₂, 0.02% BSA, 0.02% Nonidet P-40, pH 7.4). Then, histone H1-containing traces of ³²P-labeled H1 were added to the binding buffer (15-μl total volume) in the presence or absence of ParaT and incubated with the chromatin beads for 30 min at 25 °C. One unit of H1 is defined as the amount needed to increase the repeat length of chromatin from 170 to 190 bp (36).

Cell Culture and Transient Transfections—HeLa cells were grown in Dulbecco's modified Eagle's medium in the presence of 10% fetal calf serum and antibiotics. For transient transfections, HeLa cells were grown in 10-cm dishes to 50–60% confluency and transfected with 15–20 μg of DNA using the calcium phosphate method. pFLAG or pFLAG-ParaT-transfected cells were detected through cotransfection of 2–3 μg of pGFP vector. For micrococcal nuclease experiments the calcium method was modified as follows: Cells were transfected with 16 μg of DNA containing 1.5 μg of pPUR (Clontech), a plasmid that confers resistance to puromycin. After 6 h the medium was changed and cells were grown for 24 h in Dulbecco's modified Eagle's medium containing 0.25 μg/ml puromycin. The transfection efficiency ranged from 75 to 90%.

Indirect Immunofluorescence and Confocal Microscopy—A polyclonal antibody recognizing the NH₂ terminus of ParaT (peptide P1, residues 5–30) was raised in rabbits (Davids Biotechnology, Germany), and the serum was purified over P1-agarose affinity column. HeLa cells grown on coverslips were fixed with methanol at −20 °C for 5 min, followed by incubation in 3.8% paraformaldehyde for 20 min at room temperature and quenched in 50 mM ammonium chloride for 15 min. Nonspecific sites were blocked with 10% fetal calf serum in PBS, and antibody incubations were carried out for 1 h in a humidified chamber. Primary and secondary antibodies were diluted in 10% fetal calf serum. Fluorescein isothiocyanate- or TRITC-conjugated anti-rabbit IgG secondary antibodies were purchased from Dianova and used at 1:200 dilution. Coverslips were mounted in Mowiol containing 100 mg/ml 1,4-diazabicyclo[2.2.2]octane (Sigma) and viewed using a Leica TCS-SP scanning confocal microscope, equipped with an argon/krypton laser and Leica TCS software. The 488 and 568 nm wavelengths were used to excite fluorescein isothiocyanate and TRITC, respectively. Images were exported to Adobe Photoshop.

Chromatin Fractionation—Isolation of S1, S2, and P chromatin fractions from HeLa nuclei was performed according to the method of Rose and Garrard (37) with minor modifications. Briefly, HeLa cells were transfected with GFP vector or GFP-ParaT and incubated in hypotonic buffer A (20 mM Hepes, pH 7.9, 20 mM NaCl, 5 mM MgCl₂, 1 mM ATP) on ice for 15 min. After incubation, cell lysates were centrifuged at $3000 \times g$. The nuclear fraction was resuspended in 200 μl of buffer B (20 mM Hepes, pH 7.9, 0.5 mM MgCl₂, 1 mM ATP, 0.3 mM sucrose, 2 mM CaCl₂, 150 mM NaCl), and DNA content was determined in 2 M NaCl. Nuclei suspension (100 μl) containing 100 μg of DNA was incubated with 8 units of micrococcal nuclease for 10 min at 15 °C and cooled on ice for 10 min. The mixture was centrifuged at $3000 \times g$ for 5 min and 10 μl of 10× stop buffer (20 mM EDTA, 10 mM EGTA, 5% SDS) were added to the supernatant (S1 fraction). The nuclear pellet was resuspended in 100 μl of 8 mM EDTA for 15 min at 4 °C and centrifuged as above. The supernatant and the pellet were designated as S2 and P fractions, respectively. For DNA analysis, S1, S2, and P fractions were treated with 1 μg/μl RNase for 10 min at 25 °C and deproteinized with 1 μg/μl proteinase K for 2 h at 37 °C. DNA was phenol-chloroform purified, ethanol-precipitated, and analyzed on 1.3% agarose gels and ethidium bromide staining.

Sperm Chromatin Decondensation Assays—Human semen was obtained from a healthy fertile donor and was provided by the Reproduction Unit of the University Hospital of Ioannina. Sperm was kept frozen at −80 °C until use. Demembraned human sperm nuclei were prepared as described (38) and incubated with 6 μg of protein at room temperature in 10 μl of reaction mixture containing 8 mM Hepes, pH 7.5, 8 mM KCl, 2 mM MgCl₂, 200 mM sucrose, and an ATP-regeneration system. After the incubation, 1 μl of the reaction mixture was added to 1 μl of PBS containing 50% glycerol, 7.4% formaldehyde, and 5 μg/ml Hoechst

33258 on a glass slide. The DNA stained with the dye was visualized under a fluorescence microscope, and the surface area of the nuclei was measured with the AutoCAD 2000 software.

Measurement of Nuclear Surface—Sperm or HeLa cell nuclei were stained with 2.5 ng/ml Hoechst and observed under a fluorescence microscope. Immunofluorescence images were imported as TIFF files to the AutoCAD software. The perimeter of the nuclei and the surface area were measured using the spline command of the program. Spline fits a smooth curve to sequence of points within a specified tolerance. AutoCAD uses NURBS (nonuniform rational B-splines) mathematics, which stores and defines a class of curve and surface data.

Fluorescence Spectroscopy Binding Assays—H1-ParaT binding was followed by monitoring the intensity of the fluorescence emitted by the single tyrosine residue of H1. A Hitachi F-2500 fluorescence spectrophotometer, fitted with a thermostatically controlled jacketed cell holder and interfaced with a Neslab RTE-111 water-bath was used. Fluorescence emission spectra in the range 280–360 nm were recorded with an excitation wavelength of 276 nm. Purified H1 from calf thymus at an initial concentration of 15 μM was titrated with increasing amounts of a 270 μM recombinant ParaT stock solution in PBS buffer. All measurements were performed at 25 °C. After each ligand addition, the samples were left to equilibrate for 5 min before the equilibrium fluorescence readings were recorded (H1 fluorescence is quenched upon ParaT binding). The dissociation constant (K_d) for the complex was estimated by non-linear regression analysis (KaleidaGraph, Synergy Software) relating the change in H1 fluorescence intensity at 306 nm (corrected for buffer contribution and for dilution) to the total added ParaT concentration through Equation 1,

$$F = (F_0 + F_{max}[L]/K_d)/(1 + [L]/K_d) \qquad (\text{Eq. 1})$$

where F, F_o, and F_{max} are the fluorescence intensities measured at each titration point, at zero ligand concentration and at saturation, respectively, and $[L]$ is the concentration of free ligand calculated by solving the quadratic equation,

$$[L]^2 + [L]([P]_0 - [L]_0 + K_d) - K_d[L]_0 = 0 \qquad (\text{Eq. 2})$$

where $[P]_o$ and $[L]_o$ are the protein and total ligand concentrations added, respectively. The titration was repeated twice, and the R^2 values were above 0.987.

Circular Dichroism Binding Assays—Circular dichroism spectra in the Far UV range were recorded on a Jasco J-715 spectropolarimeter interfaced with a Peltier element for temperature control. The instrument was calibrated with a 0.1% aqueous solution of *d*-10-camphor sulfonic acid. Solutions of the proteins used in the fluorescence experiment were in PBS buffer, and their concentration ranged from 6 to 25 μM. Far-UV CD spectra were recorded at 25 °C, with 0.2 nm resolution, averaged over five scans, and the baseline was corrected by subtraction of the buffer spectrum at the same temperature. Quartz single-chamber cells with path lengths of 0.1 or 0.2 cm and a double-chamber cuvette with a path length of 0.4375 cm for each chamber were used (Hellma). In the latter case, a 6 μM solution of H1 in PBS was placed in one chamber and an equimolar solution of ParaT in the second, and far-UV CD spectra were recorded, corresponding to the sum of spectra of the two components. Subsequently, the contents of the two chambers were mixed and another CD spectrum was recorded. This spectrum corresponds to the mixture of the two proteins.

RESULTS

ParaT Is Localized in Distinct Nuclear Foci—Previous work has shown that ParaT is a nuclear protein associated with early replication domains, suggesting a role of this acidic polypeptide in active chromatin (39). Confocal laser scanning microscopy using affinity-purified antibodies against the NH$_2$-terminal region of ParaT revealed a nuclear punctuate staining of the endogenous protein in interphase cells (Fig. 1B, *panel a*). Interestingly, judging from the overlay of ParaT staining with propidium iodide (*PI*) that mainly decorates heterochromatin, ParaT foci were found to be scattered throughout the nucleoplasm and totally excluded from dense heterochromatic regions (*panel a*, *merge*). During prophase, where extended interphase chromatin slowly condenses into well defined chromosomes, ParaT was detected in distinct foci mainly localized in the vicinity of chromosomes (Fig. 1B, *panel b*). In late mitotic phases ParaT speckles were concentrated around the con-
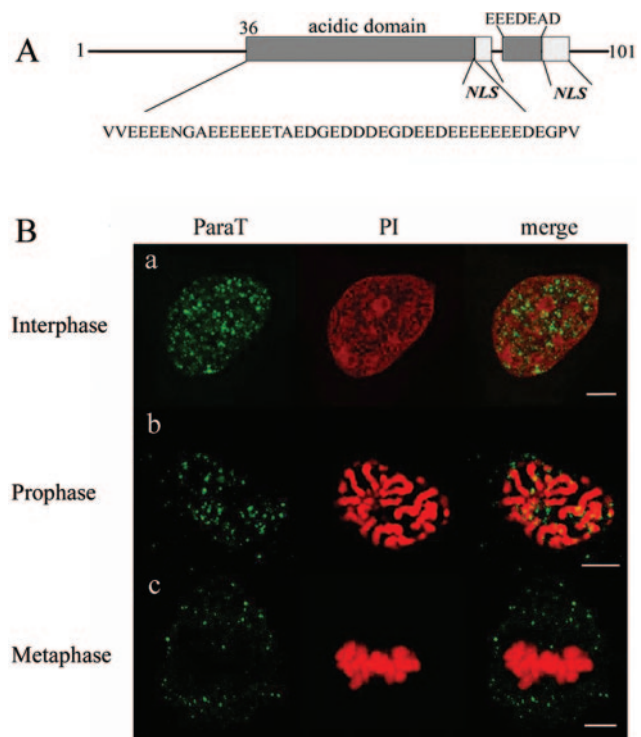

FIG. 1. **Subnuclear localization of ParaT.** *A*, schematic representation of ParaT. The polyglutamic acidic domain and the bipartite nuclear localization signal (NLS) of rat ParaT. *B*, indirect immunofluorescence and confocal scanning microscopy. HeLa cells grown on coverslips were fixed and labeled with affinity-purified anti-ParaT antibody. *ParaT*, confocal optical sections of cells labeled for endogenous ParaT at different cell cycle phases interphase (*a*), prophase (*b*), and metaphase (*c*). *PI*, DNA staining with propidium iodide. *Merge*, overlay of ParaT and PI staining. *Scale bar*, 2 μm

densed chromosomes (Fig. 1B, *panel c*). These data suggest that ParaT is mainly associated with euchromatic nucleosomal sites rather than with condensed heterochromatic regions.

ParaT Modulates the Binding of H1 to Chromatin—Our previous work has shown a specific interaction between ParaT and linker histone H1 (21). More specifically, *in vitro* binding assays under native conditions detected contacts between ParaT and the globular domain of H1 (21), a central folded region of H1 that binds four-way junction DNA (40) and protects an additional 20 bp from micrococcal nuclease digestion (6, 41). Taking into account these results, we hypothesized that ParaT might modulate the binding of H1 to chromatin. Previous studies have shown a relationship between nucleosome spacing and H1 binding to nucleosomes (8). Based on this, we first studied the effect of ParaT on the interaction of H1 with chromatin by visualizing the changes in nucleosome repeat length (NRL). Our analysis was based on a chromatin reconstitution system using extracts derived from *Drosophila* early embryos (35). Incorporation of H1 into nucleosomes in the absence of ParaT increased the NRL from 170 to 205 bp (Fig. 2A, *lanes 1* and *2*), as expected (8). However, when ParaT was added in the assembly reaction with H1, the NRL increased only to 195 bp (*lane 3*). These data support the conclusion that the H1 on the template is altered and/or bound by ParaT, such that the repeat length is changed.

To study further the effect of ParaT on H1-containing chromatin, we employed an *in vitro* chromatin reconstitution system using bead-immobilized DNA (36). Chromatin was first assembled on immobilized DNA in the presence of histone H1, and then H1 was washed off the beads with 650 mM NaCl, to create nucleosomal arrays with free H1-binding sites. Subsequently, the chromatin beads were incubated with 4 units of H1
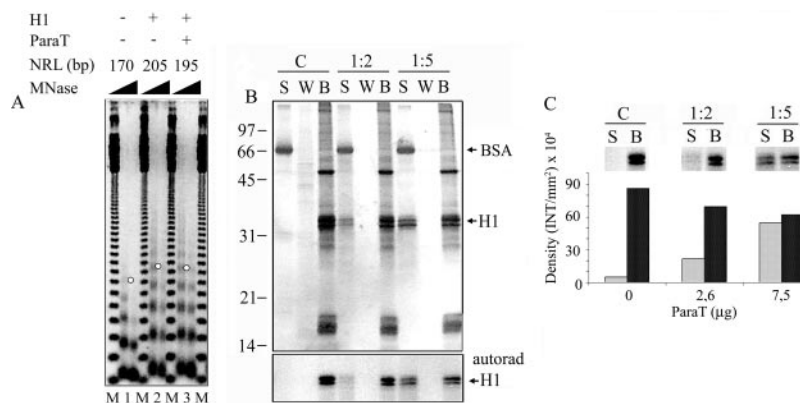
FIG. 2. **The effect of ParaT on the interaction of histone H1 with chromatin.** *A*, NRL changes. Plasmid DNA was assembled into chromatin with *Drosophila* extracts without H1 (*lane 1*) or with 2 units of histone H1 (*lanes 2* and *3*) in the absence (*lane 2*) or presence of 6 μg of ParaT (*lane 3*). Reconstituted chromatin was digested with micrococcal nuclease for 30 s or 1 min. Purified DNA was analyzed on a 1.3% agarose gel and stained with ethidium bromide. *White circles* mark the pentanucleosome-derived DNA, visualizing the change in NRL. *M*, 123-bp ladder (Invitrogen). *B*, ParaT inhibits the binding of H1 to chromatin. Chromatin with free H1 binding sites was reconstituted on immobilized DNA and then incubated with 4 units of calf histone H1 and traces of ^{32}P-phosphorylated H1, in the absence (*C*) or in the presence of ParaT (H1/ParaT ratios 1:2, 1:5 w/w). Supernatants were removed, and the beads were washed three times with the binding buffer. Supernatant (*S*), the last wash (*W*), and the beads (*B*) were analyzed by 15% SDS-PAGE. The gel was stained with silver. *Numbers* on the *left* indicate the molecular masses in kDa. *C*, quantitation of the ParaT effect on H1 binding to chromatin. The autoradiography of the gel shown in *B* was subjected to densitometry to quantitate the incorporation of H1 to nucleosomes in the presence of ParaT. The density of H1 bands (INT/mm^2) in the supernatant and chromatin beads was determined by densitometry analysis (Quantity One, Bio-Rad), and it is displayed in the graph using arbitrary units.

containing traces of ^{32}P-phosphorylated H1 in the absence or in the presence of increasing concentrations of ParaT. As depicted in Fig. 2*B*, in all cases the assembled chromatin contained the full complement of core histones. However, the binding of H1 to chromatin beads was significantly inhibited in the presence of ParaT (Fig. 2*B*, *lanes B*), with a concomitant retainment of H1 in the supernatant (*lanes S*). Quantitation of the intensity of the bands of the autoradiography by densitometry revealed that this effect was dose-dependent (Fig. 2*C*).

We next investigated the possibility that the alteration in NRL and the inhibition of H1 binding to chromatin beads in the presence of ParaT might be due to a structural change of H1 resulting from its interaction with ParaT. To this aim, we used CD spectroscopy, a technique sensitive to conformational changes and well established in the field of protein folding (42). CD spectra of purified histone H1 and recombinant ParaT were recorded (*a*) before and (*b*) after they were mixed in several molar ratios. In all cases the CD spectrum of the mixture was different from the sum of the CD spectra of the individual proteins. More specifically, the CD pattern observed for the mixture of the two proteins was distinctly indicative of a higher content of secondary structure (possibly of an α-helical type) in comparison to the CD patterns of the individual proteins and to their arithmetic sum (Fig. 3*A*). Such a difference could only result from a change in conformation of one or both proteins upon mixing. These results suggest that the interaction of the two proteins is accompanied by a conformational change, but they cannot indicate whether the conformation of one or both proteins is affected. To address this specific question we turned to fluorescence spectroscopy measurements. Both proteins are poor in aromatic amino acids: There is no such amino acid in the sequence of ParaT and only one (Tyr-70) in the sequence of the globular part of histone H1, which could serve as an intrinsic fluorescence chromophore. Previous studies indicate that Tyr-70 is buried in the hydrophobic core of the protein (43). Thus, it is reasonable to expect that any change in the fluorescence spectrum of H1 upon binding to ParaT would only result from a global rearrangement of the H1 conformation. The binding of ParaT to H1 was monitored by fluorescence spectroscopy. A clear and gradual shift of the intensity and of the wavelength of maximum fluorescence emission was observed, when increasing amounts of ParaT were added to H1 (Fig. 3*B*). Such a

shift can only result if the microenvironment of the H1 chromophore is significantly altered when ParaT is added to the solution of H1. Therefore, the fluorescence results are highly suggestive of a conformational change of H1 when it interacts with ParaT. We cannot, however, exclude the possibility that ParaT undergoes a similar change as well, which cannot be detected by our fluorescence experiments due to the lack of an intrinsic chromophore in the ParaT sequence.

The observed gradual change in fluorescence intensity of H1 upon addition of ParaT was used for a quantitative fluorescence-based binding assay. A binding curve was obtained by monitoring the change in fluorescence intensity at 306 nm as a function of ParaT concentration at constant temperature (Fig. 3*C*). Fitting of the fluorescence data resulted in a K_d value of 19.6 ± 11.3 μM for the H1-ParaT interaction. Such a modest *in vitro* affinity is not unusual for interactions between chromatin and chromatin-remodeling factors (44–46) and could be due to several reasons (see "Discussion").

ParaT Induces Global Chromatin Decondensation—Because ParaT affects the binding of H1 to nucleosomes and histone H1 is the major determinant of higher order chromatin folding (7), we investigated the effect of ParaT on chromatin structure. We used two different experimental systems: sperm chromatin as an *in vitro* system and ParaT-overproducing cells as an *in vivo* system. Sperm has an exceptionally dense chromatin packing compared with that of nuclei from somatic cells and has been used extensively in chromatin decondensation studies (38, 47). In our study, we used human sperm nuclei, which are approximately spherical compared with the spiral shape of *Xenopus* nuclei, to quantitate more accurately the extent of sperm decondensation. Demembraned human sperm nuclei were incubated with purified ParaT and the sperm decondensation factor TAF-Iβ (38) or BSA, which were used as positive and negative controls, respectively. After incubation, the DNA was stained with Hoechst 33258 and visualized under a fluorescence microscope. As shown in Fig. 4*A*, upon challenging sperm nuclei with ParaT, the nuclei displayed approximately a 2-fold increase in their surface. Using the AutoCAD 2000 software, the average surface area of 50 nuclei treated with BSA, ParaT, or TAF-1β was found to be 2.0, 3.1, and 3.2, respectively. To discriminate among different subgroups, the values of each experiment were classified arbitrarily into three clusters (1–1.5, 1.5–2, and >2),
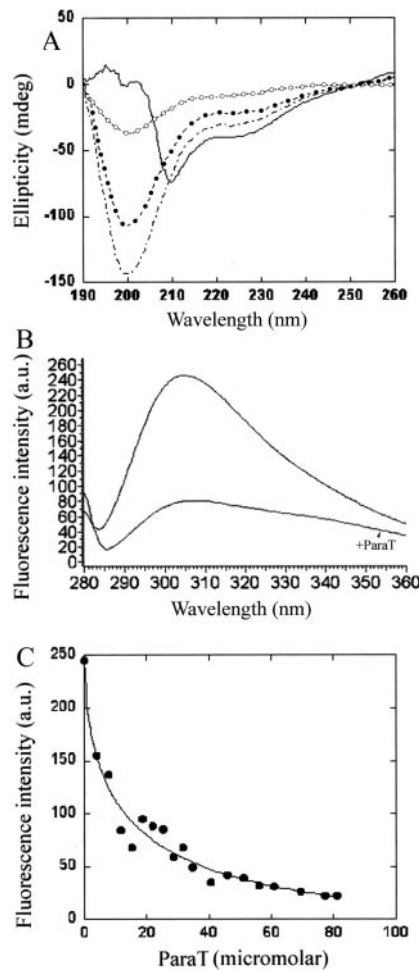
FIG. 3. **Changes of H1 conformation upon interaction with ParaT.** *A*, CD binding assays. Circular dichroism spectra of H1 (*open circles*), ParaT (*closed circles*), and of a mixture of ParaT and H1 in 3:1 molar ratio (*solid line*) protein solutions in PBS buffer. For comparison, the arithmetic sum of the H1 and ParaT spectra is also shown (*dashed-dotted line*). *B*, fluorescence emission spectra. The fluorescence emission spectra of a 15 μM solution of H1 in PBS buffer (*top*) and of the same solution after addition of a stoichiometric amount of ParaT (*bottom*). Excitation was at 276 nm. *C*, fluorescence-based binding assay. H1-ParaT binding was followed by monitoring the intensity of the fluorescence emitted at 306 nm by the single tyrosine residue of H1 after excitation at 276 nm. H1 at an initial concentration of 15 μM was titrated with increasing amounts of a 270 μM ParaT stock solution in PBS buffer. The *solid line* represents the binding curve derived by non-linear regression analysis of the fluorescence intensity values at 306 nm, corrected for dilution and for buffer contribution.

corresponding to small, medium, and large nuclear surface area. The results shown in Fig. 4*B* indicate that 50% of the nuclei treated with ParaT displayed large surface area, an effect comparable with that of TAF-1β.

We next examined whether ParaT can function as a chromatin decondensation factor *in vivo*. GFP-ParaT and FLAG-tagged ParaT expression plasmids were transiently transfected into HeLa cells and 36 h post-transfection, cells were fixed and stained with Hoechst 33258. Overexpression of ParaT resulted in enlargement of the nuclei compared with cells transfected with the control vectors with a concomitant decrease of the intensity of DNA staining (Fig. 5*A*). To quantitate this effect, we collected images of ~100 nuclei (medium or highly transfected) from each transfection experiment, and measured the surface area of the nuclei using the AutoCAD software. The average nuclei surface area of GFP-ParaT-, FLAG-ParaT-, and GFP-TAF-1β-overexpressing cells was found to be 9.1, 8.4, and 8.6, respectively. On the contrary, nontransfected cells or cells
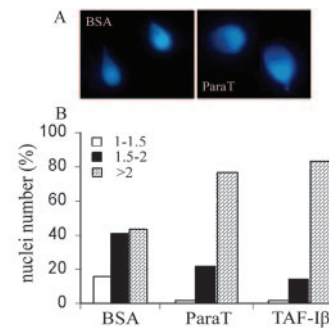

FIG. 4. **Decondensation of human sperm chromatin by ParaT.** *A*, human sperm chromatin decondensation. Sperm chromatin was incubated with 6 μg of ParaT or BSA, as described under "Materials and Methods." After incubation, aliquots were mixed with the fixation buffer containing the Hoechst dye and chromosomal DNA was visualized under a fluorescence microscope. *B*, measurements of nuclei surface. Quantitation of the nuclei surface of the experiment described in *A* with the AutoCAD 2000 software. *TAF-1β*, template-activating factor Iβ, used as positive control. Nuclei surface area values were classified arbitrarily into three groups (1–1.5, 1.5–2, and >2) to represent the extent of sperm chromatin decondensation.

transfected with empty vectors (pGFP and pFLAG) displayed an average surface nuclei area of 6.3, 5.9, and 5.8, respectively. Classification of the values arbitrarily into three groups (<6, 6–8, and >8), revealed that 80% of the cells transfected with ParaT-expressing vectors had larger nuclei, suggesting that ParaT exhibits chromatin decondensation activity *in vivo* (Fig. 5*B*).

In another attempt to study the effect of ParaT on chromatin structure, we tried to partition between active and inactive chromatin, using an established fractionation procedure in which nuclei are subjected to mild digestion with micrococcal nuclease and subsequent extraction with EDTA (37). This method sequentially yields three fractions that contain material that is soluble in divalent metals (S1) and soluble in EDTA (S2) and a remaining insoluble fraction (P). The detailed analysis of the protein components of these fractions has shown that S1 is highly depleted of H1 relative to S2, which contains more compact chromatin, whereas the nuclease-resistant fraction P is enriched in actively transcribed gene sequences and contains nuclear matrix components (37, 48). In accordance with this protocol, HeLa cells overexpressing GFP-ParaT or GFP alone were incubated with micrococcal nuclease and centrifuged to obtain the supernatant fraction (S1). Subsequently, the pellet was resuspended in an EDTA-containing buffer and centrifuged to prepare S2 and the remaining insoluble fraction P. As shown by DNA analysis on agarose gels, the profile of micrococcal nuclease digestion of S1 and S2 fractions was similar in both cell populations (Fig. 5*C*, *lanes 1–5*). However, the DNA extracted from the nuclease-resistant chromatin fraction (P) of ParaT-overproducing cells yielded a typical nucleosomal ladder with a strong mono-nucleosomal band (Fig. 5*C*, *lane 7*). On the contrary, the corresponding fraction of DNA obtained from control cells was more heterogenous and exhibited a smeared profile (Fig. 5*C*, *lane 6*). Taken together, these results suggest the involvement of ParaT in the decondensation of chromatin fibers.

DISCUSSION

ParaT belongs to a group of acidic proteins that interact specifically with linker histone H1 *in vitro* and *in vivo* (21). In the present study, the effect of ParaT on the interaction of histone H1 with chromatin was studied using a cell-free chromatin reconstitution system on bead-immobilized DNA (36). This chromatin system assembles regularly spaced nucleosomes on DNA attached to paramagnetic beads with or without
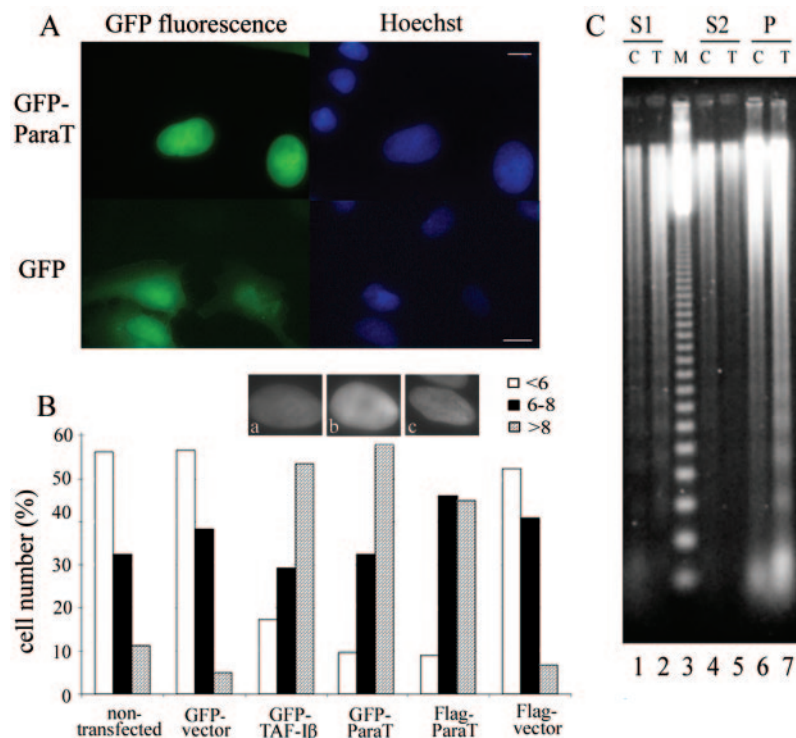
Fig. 5. **ParaT induces global chromatin decondensation.** *A*, overexpression of ParaT in HeLa cells. Cells were transiently transfected with pGFP-ParaT or pGFP. 36 h post-transfection cells were fixed, stained with Hoechst, and observed under a fluorescence microscope. *Left*, GFP fluorescence; *right*, DNA staining. *Scale bar*, 10 μm. *B*, measurements of nuclei surface. HeLa cells were transiently transfected with pGFP, pGFP-TAF-Iβ, pGFP-ParaT, pFLAG-ParaT, and pFLAG expression plasmids, as indicated. pFLAG-ParaT- and pFLAG-transfected cells were detected through cotransfection of pGFP expression vector. *Upper panel*, immunofluorescence images showing the nuclear localization of GFP-TAF-Iβ (*a*), GFP-ParaT (*b*), and FLAG-ParaT (*c*). *Lower panel*, the surface area of transfected nuclei was measured with the AutoCAD 2000 software, and the values were classified arbitrarily into three groups (4–6, 6–8, and >8). *C*, chromatin fractionation. Nuclei were prepared from pGFP- or pGFP-ParaT-transfected HeLa cells, digested with micrococcal nuclease, and separated into supernatant (*S1*) and pellet, as described under "Materials and Methods." The pellet was extracted with EDTA and centrifuged to yield supernatant (*S2*) and (*P*) chromatin fractions. The fractions were deproteinized and analyzed by agarose gel electrophoresis and ethidium bromide staining. In *C*: *T* indicates DNA obtained from HeLa cells transfected with pGFP or pGFP-ParaT, respectively. *M*, 123-bp ladder (Invitrogen).

H1 and offers the opportunity to study the interaction of H1 with nucleosomes under different salt conditions and in the presence of several factors (36). Our results show that ParaT was able to inhibit the association of H1 with the chromatin template. Remarkably, the presence of this acidic protein during chromatin assembly resulted in the organization of H1-containing chromatin with reduced nucleosomal spacing.

To provide interpretation for these data, one should take into consideration the binding determinants of H1 interaction with chromatin and the sequence characteristics of ParaT. Previous studies have clearly established that the interaction of H1 with chromatin is dynamic and the overall affinity is governed by a set of interactions mediated by the globular domain (49, 50) and the positively charged COOH-terminal tail (51, 52). The folded globular domain of H1 binds preferentially to crossovers of duplex strands in superhelical DNA (40), contains two binding sites for DNA (49), and protects an additional 20 bp from micrococcal nuclease digestion (6, 41). The highly basic COOH-terminal domain of H1 adopts secondary α-helical structure upon binding to DNA (51) and has been identified as the primary determinant of H1 binding to chromatin *in vitro* (51, 53) and *in vivo* (52). Interestingly, molecular modeling of the chromatosome particle predicts that the location of the COOH-terminal domain onto the particle is directed by the positioning of the globular region (54). Based on our results, it is appealing to propose that the binding of ParaT within the globular domain of H1 affects the conformation of the linker histone in such a way that the binding affinity of H1 for chromatin is altered. The CD-based results indicate a higher content of secondary structure when the two proteins are mixed, whereas the fluorescence data confirm that the conformation of H1 is definitely affected by the interaction of the two proteins. This increased amount of helicity that seems to result from the binding is highly reminiscent of the behavior of the H1 C terminus that becomes folded (α-helical) when it binds to linker DNA and it might provide a clue for the possible mechanism of inhibition of H1-chromatin interaction by ParaT. On the other hand, ParaT exhibits all the characteristics of "natively disordered" proteins (55), which have structural plasticity and can accommodate different shapes upon association with several partners; it is highly polar, showing low structural complexity at neutral pH and becomes partially folded at low pH (data not shown), possibly due to the decrease of charge and minimization of charge/charge interactions under acidic conditions. Such a protein is reasonably expected to be involved in highly dynamic interactions. Our model implies that ParaT might be associated with chromatin transiently through cycles of binding and release. Such a dynamic interaction might not be detectable with our experimental system, and this provides a possible explanation to the fact that the protein was not detected on chromatin beads (not shown). In addition, the relatively moderate affinity of the H1-ParaT interaction, estimated from our fluorescence measurements, which is not unusual for interactions between chromatin and nuclear proteins (44–46), points to two nonmutually exclusive possibilities. First, it could suggest that other additional factors might be involved in stabilizing these interactions *in vivo*. Second, it might indicate that the biologically important but suboptimal H1-ParaT interaction can occur only if the local concentration is high enough. Interestingly, both possibilities are perfectly consistent with

the ample evidence for the localization of ParaT in specific subnuclear domains. In short, taken together, our data suggest that ParaT may regulate the mode of H1 association with chromatin regions.

There are several potential consequences of reducing H1 content in chromatin, either at the level of the nucleosome or globally, at the level of the cell nucleus, which arise from the ability of H1 to compact chromatin (7). We have obtained experimental evidence for a role of ParaT in chromatin decondensation using human sperm chromatin as an *in vitro* model system. Sperm chromatin represents a physiological highly condensed chromatin template, compared with the *in vitro* reconstituted chromatin substrates, which do not reproduce the higher order nature of chromatin of the interphase nuclei. Early experiments have investigated in detail the decondensation of sperm chromatin upon incubation with acidic proteins. For example, substantial swelling of nuclei was observed when sperm was challenged with TAF-I β sperm decondensation factor (38) or nucleoplasmin, a highly acidic, histone-binding protein in *Xenopus* egg extracts (47). Interestingly, ParaT resembles both nucleoplasmin and TAF-I β with respect to its central region that contains the polyglutamic stretch, which suggests similar functions of these proteins. In our study we used human sperm nuclei, which have round morphology and allow an accurate quantification of nuclear surface. Our results indicated that ~50% of the sperm nuclei were highly decondensed upon challenging with ParaT.

Consistent with the *in vitro* data, overexpression of ParaT in HeLa cells resulted in an increase of cell nuclei surface, suggesting global chromatin decondensation. Interestingly, and in agreement with these results, disruption of the gene encoding macronuclear histone H1 of *Tetrahymena* resulted in enlarged macronuclei, presumably due to lower levels of chromatin compaction (56). The decondensation state of chromatin in the cells that overproduce ParaT was further confirmed by micrococcal nuclease digestion of chromatin fractions. It is well established that partial digestion of chromatin by micrococcal nuclease yields a "ladder" of oligonucleosome-sized fragments that reflects the extent of chromatin accessibility to enzymatic digestion. In our experimental system, micrococcal nuclease "ladders" were evident in the fraction that contained nuclease-resistant chromatin from ParaT-overproducing cells. Interestingly, nuclease-resistant chromatin has been proposed to be a component of the nuclear matrix that contains active genes, RNA polymerase (37, 48), and the human SWI/SNF chromatin remodeling complex (57), suggesting a potential function of ParaT in active chromatin.

In summary, the results reported here introduce ParaT as a new member of the group of proteins that modulate H1 interaction with chromatin and affect the condensation state of chromatin fibers. ParaT localizes in subnuclear domains, indicating that its local concentration is significantly higher at specific chromatin regions. Recent evidence has shown that some of the subnuclear bodies contain factors involved in the processing and transcription of RNA, whereas others function either as depots supplying factors to active gene loci, or platforms accumulating factors involved in replication or transcription (58). Therefore, identification of functionally relevant neighboring proteins that reside at ParaT domains will provide further insight into the molecular mechanism of this nuclear polypeptide. Nevertheless, the punctuated nuclear pattern guarantees a temporally and spatially coordinated availability of ParaT to perform optimally its function. Interestingly, fluorescence recovery after photobleaching experiments reveal that ParaT moves very fast throughout the cell nucleus (not shown). Because H1 has rapid dynamics of association and dissociation (59), ParaT may access the linker histone in nucleosomes rapidly and modulate the dynamic interaction of H1 with chromatin, either globally or locally. It is worth mentioning at this point that such a dynamic association is perfectly consistent with the modest affinity detected by our fluorescence binding experiments. A similar modest affinity (10 μM) has been reported for an intramolecular interaction closely resembling that of ParaT-H1, namely the one between the acidic tail and a part (boxA) of high mobility group box 1 (HMGB1) protein (46). The acidic tail is believed to modulate the interaction of HMGB1 with nucleosomes and chromatin remodeling machines (60, 61). This function of the tail is due to its extended and flexible structure that interacts with specific residues within and between high mobility group boxes, shielding part of the protein surface from other interactions in a dynamic way (46).

The structural and functional significance of varying histone H1 stoichiometry in chromatin has been recently the focus of intensive work. Because linker histone binding to chromatin stabilizes folded secondary structures (7, 62), the H1-nucleosome interactions are greatly altered in active chromatin (7, 63). Consistent with this, accessible chromatin at a glucocorticoid-responsive enhancer was found to be associated with a decreased interaction of linker H1 with DNA (64). Furthermore, mouse embryos lacking three mouse H1 subtypes (H1c, H1d, and H1e) die by mid gestation, suggesting that changes in H1 stoichiometry are crucial for proper embryonic development (65). Therefore, variations in H1 stoichiometry may indicate distinct chromatin higher order structures and functional states. Competition between H1 and other nuclear proteins containing long acidic stretches, such as high mobility group proteins (66) and prothymosin α (26), has been recently reported. The effects of these proteins on the binding of H1 to chromatin might be either additive or synergistic depending on temporal/spatial localization to specific chromatin loci and the tissue-specific or developmental-specific protein expression patterns. We speculate that ParaT may participate in global chromatin remodeling during gene activation and perhaps the transcription initiation process itself. Further studies using small interfering RNAs and chromatin immunoprecipitation assays will shed light on the role of ParaT in gene regulation and may lead to the identification of specific genes that are regulated by changes of H1 stoichiometry.

REFERENCES

1. van Holde, K. E. (1988) *Chromatin*, Springer Verlag, New York
2. Fedor, M. J. (1992) *Curr. Opin. Cell Biol.* **4,** 436–443
3. Felsenfeld, G. (1992) *Nature* **355,** 219–224
4. Mizzen, C. A., and Allis, C. D. (2000) *Science* **289,** 2290–2291
5. Luger, K., Mader, A. W., Richmond, R. K., Sargent, D. F., and Richmond, T. J. (1997) *Nature* **389,** 251–260
6. van Holde, K., and Zlatanova, J. (1996) *Proc. Natl. Acad. Sci. U. S. A.* **93,** 10548–10555
7. Carruthers, L. M., Bednar, J., Woodcock, C. L., and Hansen, J. C. (1998) *Biochemistry* **37,** 14776–14787
8. Blank, T. A., and Becker, P. B. (1995) *J. Mol. Biol.* **252,** 305–313
9. Pennings, S., Meersseman, G., and Bradbury, E. M. (1994) *Proc. Natl. Acad. Sci. U. S. A.* **91,** 10275–10279
10. Juan, L. J., Utley, R. T., Vignali, M., Bohm, L., and Workman, J. L. (1997) *J. Biol. Chem.* **272,** 3635–3640
11. Gunjan, A., Sittman, D. B., and Brown, D. T. (2001) *J. Biol. Chem.* **276,** 3635–3640
12. Hill, D. A., and Imbalzano, A. N. (2000) *Biochemistry* **39,** 11649–11656
13. Horn, P. J., Carruthers, L. M., Logie, C., Hill, D. A., Solomon, M. J., Wade, P. A., Imbalzano, A. N., Hansen, J. C., and Peterson, C. L. (2002) *Nat. Struct. Biol.* **9,** 263–267
14. Thomas, J. O. (1999) *Curr. Opin. Cell Biol.* **11,** 312–317
15. Zlatanova, J., Caiafa, P., and Van Holde, K. (2000) *FASEB J.* **14,** 1697–1704

16. Shen, X., and Gorovsky, M. A. (1996) *Cell* **86,** 475–483
17. Doenecke, D., Albig, W., Bode, C., Drabent, B., Franke, K., Gavenis, K., and Witt, O. (1997) *Histochem. Cell Biol.* **107,** 1–10
18. Alami, R., Fan, Y., Pack, S., Sonbuchner, T. M., Besse, A., Lin, Q., Greally, J. M., Skoultchi, A. I., and Bouhassira, E. E. (2003) *Proc. Natl. Acad. Sci. U. S. A.* **100,** 5920–5925
19. Lee, H., Habas, R., and Abate-Shen, C. (2004) *Science* **304,** 1675–1678
20. Konishi, A., Shimizu, S., Hirota, J., Takao, T., Fan, Y., Matsuoka, Y., Zhang, L., Yoneda, Y., Fujii, Y., Skoultchi, A. I., and Tsujimoto, Y. (2003) *Cell* **114,** 673–688
21. Kondili, K., Tsolas, O., and Papamarcaki, T. (1996) *Eur. J. Biochem.* **242,** 67–74
22. Clinton, M., Frangou-Lazaridis, M., Panneerselvam, C., and Horecker, B. L. (1989) *Arch. Biochem. Biophys.* **269,** 256–263
23. Frangou-Lazaridis, M., Clinton, M., Goodall, G. J., and Horecker, B. L. (1988) *Arch. Biochem. Biophys.* **263,** 305–310
24. Trompeter, H. I., Blankenburg, G., Brugger, B., Menne, J., Schiermeyer, A., Scholz, M., and Soling, H. D. (1996) *J. Biol. Chem.* **271,** 1187–1193
25. Clinton, M., Frangou-Lazaridis, M., Panneerselvam, C., and Horecker, B. L. (1989) *Biochem. Biophys. Res. Commun.* **158,** 855–862
26. Karetsou, Z., Sandaltzopoulos, R., Frangou-Lazaridis, M., Lai, C. Y., Tsolas, O., Becker, P. B., and Papamarcaki, T. (1998) *Nucleic Acids Res.* **26,** 3111–3118
27. Karetsou, Z., Kretsovali, A., Murphy, C., Tsolas, O., and Papamarcaki, T. (2002) *EMBO Rep.* **3,** 361–366
28. Martini, P. G., Delage-Mourroux, R., Kraichely, D. M., and Katzenellenbogen, B. S. (2000) *Mol. Cell. Biol.* **20,** 6224–6232
29. Cotter, M. A., 2nd, and Robertson, E. S. (2000) *Mol. Cell. Biol.* **20,** 5722–5735
30. Brand, I. A., and Heinickel, A. (1991) *J. Biol. Chem.* **266,** 20984–20989
31. Trompeter, H. I., Brand, I. A., and Soling, H. D. (1989) *FEBS Lett.* **253,** 63–66
32. Okamoto, K., and Isohashi, F. (2000) *Eur. J. Biochem.* **267,** 155–162
33. Sambrook, J., Fritsch, E. F., and Maniatis, T. (1989) *Molecular Cloning: A Laboratory Manual*, 3rd Ed., Cold Spring Harbor Laboratory Press, Cold Spring Harbor, NY
34. Haritos, A. A., Salvin, S. B., Blacher, R., Stein, S., and Horecker, B. L. (1985) *Proc. Natl. Acad. Sci. U. S. A.* **82,** 1050–1053
35. Becker, P. B., Tsukiyama, T., and Wu, C. (1994) *Methods Cell Biol.* **44,** 207–223
36. Sandaltzopoulos, R., Blank, T., and Becker, P. B. (1994) *EMBO J.* **13,** 373–379
37. Rose, S. M., and Garrard, W. T. (1984) *J. Biol. Chem.* **259,** 8534–8544
38. Matsumoto, K., Nagata, K., Miyaji-Yamaguchi, M., Kikuchi, A., and Tsujimoto, M. (1999) *Mol. Cell. Biol.* **19,** 6940–6952
39. Vareli, K., Frangou-Lazaridis, M., van der Kraan, I., Tsolas, O., and van Driel, R. (2000) *Exp. Cell Res.* **257,** 152–161
40. Varga-Weisz, P., Zlatanova, J., Leuba, S. H., Schroth, G. P., and van Holde, K. (1994) *Proc. Natl. Acad. Sci. U. S. A.* **91,** 3525–3529
41. An, W., Leuba, S. H., van Holde, K., and Zlatanova, J. (1998) *Proc. Natl. Acad. Sci. U. S. A.* **95,** 3396–3401
42. Greenfield, N. J. (2004) *Methods Mol. Biol.* **261,** 55–78
43. Giancotti, V., Quadrifoglio, F., Cowgill, R. W., and Crane-Robinson, C. (1980) *Biochim. Biophys. Acta* **624,** 60–65
44. Jacobs, S. A., Taverna, S. D., Zhang, Y., Briggs, S. D., Li, J., Eissenberg, J. C., Allis, C. D., and Khorasanizadeh, S. (2001) *EMBO J.* **20,** 5232–5241
45. Nielsen, P. R., Nietlispach, D., Mott, H. R., Callaghan, J., Bannister, A., Kouzarides, T., Murzin, A. G., Murzina, N. V., and Laue, E. D. (2002) *Nature* **416,** 103–107
46. Knapp, S., Muller, S., Digilio, G., Bonaldi, T., Bianchi, M. E., and Musco, G. (2004) *Biochemistry* **43,** 11992–11997
47. Dingwall, C., Dilworth, S. M., Black, S. J., Kearsey, S. E., Cox, L. S., and Laskey, R. A. (1987) *EMBO J.* **6,** 69–74
48. Kreitz, S., Ritzi, M., Baack, M., and Knippers, R. (2001) *J. Biol. Chem.* **276,** 6337–6342
49. Goytisolo, F. A., Gerchman, S. E., Yu, X., Rees, C., Graziano, V., Ramakrishnan, V., and Thomas, J. O. (1996) *EMBO J.* **15,** 3421–3429
50. Ramakrishnan, V., Finch, J. T., Graziano, V., Lee, P. L., and Sweet, R. M. (1993) *Nature* **362,** 219–223
51. Lu, X., and Hansen, J. C. (2004) *J. Biol. Chem.* **279,** 8701–8707
52. Hendzel, M. J., Lever, M. A., Crawford, E., and Th'ng, J. P. (2004) *J. Biol. Chem.* **279,** 20028–20034
53. Allan, J., Hartman, P. G., Crane-Robinson, C., and Aviles, F. X. (1980) *Nature* **288,** 675–679
54. Bharath, M. M., Chandra, N. R., and Rao, M. R. (2003) *Nucleic Acids Res.* **31,** 4264–4274
55. Dunker, A. K., Lawson, J. D., Brown, C. J., Williams, R. M., Romero, P., Oh, J. S., Oldfield, C. J., Campen, A. M., Ratliff, C. M., Hipps, K. W., Ausio, J., Nissen, M. S., Reeves, R., Kang, C., Kissinger, C. R., Bailey, R. W., Griswold, M. D., Chiu, W., Garner, E. C., and Obradovic, Z. (2001) *J. Mol. Graph. Model* **19,** 26–59
56. Shen, X., Yu, L., Weir, J. W., and Gorovsky, M. A. (1995) *Cell* **82,** 47–56
57. Reyes, J. C., Muchardt, C., and Yaniv, M. (1997) *J. Cell Biol.* **137,** 263–274
58. Lamond, A. I., and Earnshaw, W. C. (1998) *Science* **280,** 547–553
59. Misteli, T., Gunjan, A., Hock, R., Bustin, M., and Brown, D. T. (2000) *Nature* **408,** 877–881
60. Bonaldi, T., Langst, G., Strohner, R., Becker, P. B., and Bianchi, M. E. (2002) *EMBO J.* **21,** 6865–6873
61. Travers, A. A. (2003) *EMBO Rep.* **4,** 131–136
62. Bednar, J., Horowitz, R. A., Grigoryev, S. A., Carruthers, L. M., Hansen, J. C., Koster, A. J., and Woodcock, C. L. (1998) *Proc. Natl. Acad. Sci. U. S. A.* **95,** 14173–14178
63. Thoma, F., Koller, T., and Klug, A. (1979) *J. Cell Biol.* **83,** 403–427
64. Flavin, M., Cappabianca, L., Kress, C., Thomassin, H., and Grange, T. (2004) *Mol. Cell. Biol.* **24,** 7891–7901
65. Fan, Y., Nikitina, T., Morin-Kensicki, E. M., Zhao, J., Magnuson, T. R., Woodcock, C. L., and Skoultchi, A. I. (2003) *Mol. Cell. Biol.* **23,** 4559–4572
66. Catez, F., Yang, H., Tracey, K. J., Reeves, R., Misteli, T., and Bustin, M. (2004) *Mol. Cell. Biol.* **24,** 4321–4328